

Modifications to ideal stability by kinetic effects in NSTX

This content has been downloaded from IOPscience. Please scroll down to see the full text.

View [the table of contents for this issue](#), or go to the [journal homepage](#) for more

Download details:

IP Address: 198.125.231.237

This content was downloaded on 02/11/2015 at 17:46

Please note that [terms and conditions apply](#).

Modifications to ideal stability by kinetic effects in NSTX

J.W. Berkery¹, S.A. Sabbagh¹, R.E. Bell², S.P. Gerhardt², B.P. LeBlanc²
and J.E. Menard²

¹ Department of Applied Physics and Applied Mathematics, Columbia University, New York, NY 10027, USA

² Princeton Plasma Physics Laboratory, Princeton University, Princeton, NJ 08544, USA

E-mail: jberkery@pppl.gov

Received 23 July 2015, revised 14 September 2015

Accepted for publication 9 October 2015

Published 30 October 2015



Abstract

Marginal stability points of global modes during high plasma pressure operation in the National Spherical Torus Experiment (NSTX) device can be found by computing kinetic modifications to ideal magnetohydrodynamic limits on stability. Calculations with the DCON code for nearly five thousand experimental equilibria show that previous estimates of the no-wall limit (below which the ideal kink/ballooning mode would be stable even without conducting structure surrounding the plasma) on the plasma beta (a ratio of plasma pressure to magnetic pressure) and internal inductance (a measure of the current profile peakedness) were relatively accurate, though about 10% low. The no-wall beta limit also decreased with increasing aspect ratio and increasing broadness of the pressure profile, and these dependencies have implications for the upgrade to NSTX which has a larger aspect ratio and new neutral beams that may increase the broadness of pressure and current profiles. Kinetic modifications to ideal limits calculated with the Modifications to Ideal Stability by Kinetic effects (MISK) code are further validated by detailed comparison with experimental results from NSTX. In several discharges the code predicts a transition from damping of the mode to growth as the time approaches the experimental time of marginal stability to the resistive wall mode (RWM). The main stabilization mechanism is through rotational resonances with the motions of thermal particles in the plasma, though energetic particles also contribute to stability, and it is often when the plasma rotation falls in between these resonances that the RWM was destabilized in NSTX. The calculations are found to be slightly affected by changing the assumed magnetic structure of the mode as well. These validations are important for real-time assessment of stability limits for disruption avoidance, and reliable projections of the stability of future devices.

Keywords: plasma stability, ideal stability, no-wall limit, resistive wall mode, kinetic effects

(Some figures may appear in colour only in the online journal)

I. Introduction

Fusion plasmas at high pressure are subject to modes of instability which can lead to disruption of the plasma [1]. One such mode is the resistive wall mode (RWM) [2–4], so called because the conducting structure surrounding the plasma slows the growth rate of the mode (γ) to a time scale associated with the penetration of a ballooning or kinking magnetic field through the resistive wall (τ_w).

RWM marginal stability is determined by a combination of ideal and kinetic effects, and determination of γ will rely upon validated reduced physics models of both. Reliable prediction of the stability of these modes can be used as a critical element for disruption avoidance in present and future devices. Specifically, reduced stability models could be developed that could employ real-time measurements (of rotation, for example) and actuation (rotation control via magnetic braking or changing neutral beam sources)

to detect approaches to marginal stability and return the plasma to a more stable state.

The national spherical torus experiment (NSTX) [5] is a compact, low aspect ratio plasma confinement device with copper stabilizing plates that is able to reach high plasma pressures and therefore is a good facility for studying the stability of the RWM. When characterized by the ratio of plasma pressure to magnetic pressure known as β , NSTX was able to access high toroidal beta, $\beta_t \equiv 2\mu_0\langle p \rangle / B_0^2$ up to 39%, and high normalized beta, $\beta_N \equiv 10^8 \langle \beta_t \rangle a B_0 / I_p$ up to 7.4 [6]. Here, p is the plasma pressure, B_0 is the vacuum toroidal field at the plasma geometric center, a is the plasma minor radius at the midplane, I_p is the plasma current and $\langle \rangle$ represents a volume average. Low aspect ratio spherical tori can reach relatively high values of β_N before the plasmas become unstable [7–9]. Next-step spherical tokamaks [10] aim to operate at high β_N for fusion performance and high non-inductive current fraction for continuous operation. This second requirement necessitates a high bootstrap current fraction, which gives a broad current profile and in turn means these plasmas will have a low internal inductance, $l_i \equiv \langle B_p^2 \rangle / \langle B_p \rangle^2$ (where B_p is the poloidal magnetic field).

From an ideal magnetohydrodynamic (MHD) stability [11, 12] standpoint, high β_N , low l_i operation is unfavorable because there theoretically exists a limit on the achievable β_N before the ideal kink/ballooning mode is unstable and growing, and this limit decreases proportionally to decreasing l_i at low l_i [13–15]. In practice, above this so-called no-wall limit, $\beta_N^{\text{no-wall}}$, the growth of the ideal kink mode is slowed to the time scale τ_w , and is converted to the RWM. Furthermore, experimental operation above the no-wall limit without active feedback control [16] has been demonstrated [3] and can be explained by the stabilizing kinetic rotational resonances [17–23]. The present work substantially extends the experimental validation of the kinetic RWM stability limit by expanding the scope of both the ideal and kinetic elements of the stability analysis and by comparison to NSTX experiments.

In NSTX the ideal MHD stability no-wall limit was first calculated by extrapolating initial equilibria to higher β (and was found to be $\beta_N \approx 4.5\text{--}4.7$) [24] and was further refined over the years by calculations using real experimental high- β equilibria, as will be presented here, and was finally characterized by $\beta_N = 4.3$ above $l_i = 0.64$ and by $\beta_N/l_i = 6.7$ from $l_i \approx 0.4$ to 0.64 [25]. Historically, NSTX operation steadily improved performance over the years first approaching, and then expanding well above the no-wall limit (see, for example, figures 3 and 14 of [7], 8(a) of [26], 2 of [27], 1 of [9], 12(a) of [28], and 15 of [25]). Values of β_N/l_i of 11 were consistently achieved without active RWM control, and $\beta_N/l_i > 13$ was achieved with active control [25].

It was also noted that the highest values of β_N/l_i were *not* the least stable. In the overall database of NSTX disruptions, disruptivity tended to decrease as β_N/l_i increased [29], disruptions due to RWMs occurred more frequently at intermediate values of β_N/l_i [25], and when low frequency MHD spectroscopy measurements via resonant field amplification (RFA) [30] were used as a tool to provide a direct measurement

of RWM stability in NSTX, stability tended to increase at the highest β_N/l_i [31]. The latter trend was explained again by kinetic stabilization effects, specifically broad rotational resonances, which modify ideal stability [31]. Additionally, plasma response to external magnetic fields (also via RFA) was shown to not increase without bound at the no-wall limit as ideal MHD stability would predict, but rather increase monotonically, as can be explained by kinetic effects (also in the DIII-D tokamak [32, 33]). Finally, the higher with-wall limit where the ideal kink is unstable even with a conducting wall was also shown to be modified by both fluid rotational and kinetic effects in NSTX [34].

Plasmas can operate stably above ideal magnetohydrodynamic limits to the pressure by dissipating the energy of the perturbed magnetic field into the motions of the particles via stabilizing rotational resonances. This modification to ideal stability by kinetic effects is calculated by various codes including the Modifications to Ideal Stability by Kinetic effects (MISK) code [35] which has been extensively developed through theory [17, 36–39] and benchmarked against other leading codes [40]. The predicted RWM growth rates have then been compared extensively to experimental results in both the National Spherical Torus Experiment (NSTX) [6, 20, 25, 31, 41] and the DIII-D tokamak [21, 42].

The details of MISK code calculations of the change in potential energy due to the perturbed kinetic pressure δW_K , which is solved using the perturbed distribution function from the drift kinetic equation, have been extensively outlined previously [17, 41] and will not be repeated in such detail here. However, we will note that MISK solves for the complex growth rate of the RWM through the dispersion relation $(\gamma - i\omega_r)\tau_w = -(\delta W_\infty + \delta W_K)/(\delta W_b + \delta W_K)$, where ω_r is the real frequency of the mode and δW_∞ is the sum of the plasma fluid and vacuum perturbed potential energies when the wall is placed at infinity and δW_b is the sum when the wall is placed at a specific location b . Both of the fluid δW terms, as well as the displacement eigenfunction ξ_\perp which is used in the MISK calculation of δW_K , are obtained from the ideal stability code PEST [43]. Calculation of the term δW_K involves a frequency resonance fraction $\lambda \propto (\omega_D + \omega_b - i\nu_{\text{eff}} + \omega_E - \omega_r - i\gamma)^{-1}$, where ω_E , the $E \times B$ frequency, scales with the plasma rotation, which is in resonance with the precession (ω_D) and bounce (ω_b) motions of the particles [20] and is effected by the collisionality (ν_{eff}) [37].

Overall, knowledge of the ideal MHD stability is insufficient to understand stability in tokamaks, but it is nevertheless informative as RWMs are still generally only expected to occur above the no-wall limit, and ideal fluid stability terms still underlie the necessary kinetic modifications. Therefore a real-time estimate of the no-wall limit is also useful for future disruption avoidance systems. To determine the marginal point accurately requires confidence in the ideal as well as the kinetic components. In a future real-time system, the ideal terms δW_∞ and δW_b might be parameterized by real-time measurements of β_N/l_i , pressure peaking, and aspect ratio (for example) rather than determined by full calculation of ideal stability codes such as PEST. Meanwhile, the kinetic term δW_K might be determined by a reduced kinetic model

dependent upon rotation, collisionality, and energetic particle fraction (for example) rather than full MISHK calculations. This emphasizes the importance of the full kinetic RWM stability analysis presented, as it is required to create quantitatively accurate reduced stability models, or stability maps, for real-time use.

The present work is outlined as follows. First, in section II we examine in detail the ideal MHD limits on stability in NSTX. Second, in section III we provide further validation of the kinetic RWM stability theory calculations against experimental NSTX unstable points, including energetic particle effects, and we examine the effect of the rotation profile and the sensitivity of the calculations to changes in the mode eigenfunction. This validation of code calculations against present experimental results is crucial for projecting the stability of future devices and for the development of real-time stability evaluation. Experimentally validated predictive capabilities and control of deleterious transient events are two areas that have been identified as the highest priority research for the future of fusion energy sciences.

II. The ideal MHD no-wall stability limit of NSTX

The DCON ideal MHD stability code [44] has been used to analyze a large database of stable NSTX equilibria. DCON calculates the change in potential energy in the plasma fluid and vacuum due to a displacement ξ . If any small displacement from the equilibrium can be found that causes the potential energy to decrease and the displacement to grow exponentially in time, then that equilibrium is ideally unstable. As an input to DCON, the NSTX equilibria were computed with the EFIT code implementation for NSTX [24] using magnetics, a diamagnetic loop measurement, and Thomson scattering profiles of the electron density and temperature [45] to partially constrain the pressure profile [9].

For toroidal mode number $n = 1$ and without any wall in the calculation, crossing from positive to negative $\delta W_{\text{no-wall}}^{n=1}$ in DCON defines exceeding the $n = 1$ no-wall limit. In the following, for clarity, we have plotted the quantity $-\delta W_{\text{no-wall}}^{n=1}$ so that negative is ‘below’ (indicated with blue dots) and positive is ‘above’ the no-wall limit (indicated with red x’s). In order to avoid the well known issue of equilibrium edge truncation in stability calculations [46, 47], we have run DCON in a consistent way by truncating the edge at the last integral safety factor $q = X$ plus 0.1 while maintaining magnetic flux less than $\Psi_{\text{high}} = 0.992$. Other sources of uncertainty in the DCON calculation include uncertainties in the equilibrium reconstruction, from measured quantities. The equilibria that were used are from a subset of the disruptivity database of NSTX discharges used in [29]. In this analysis, equilibria were taken from periods during the plasma current steady-state and that had $\beta_N/l_i > 2.5$. Central safety factor $q_0 < 1$ can affect the stability limit calculation and these cases were not specifically excluded, but it is extremely rare for NSTX equilibria in the flattop to have $q_0 < 1$. This is a well-known aspect of H-mode

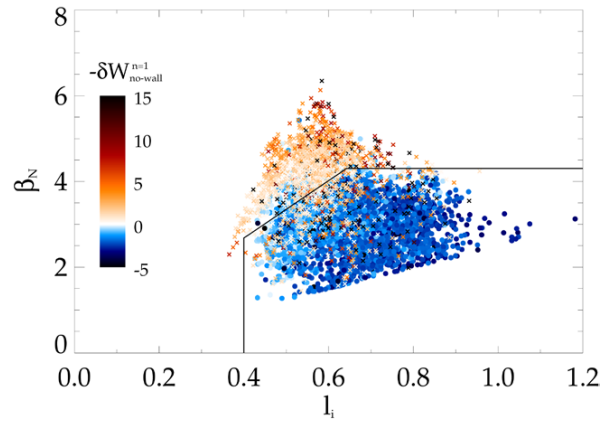


Figure 1. The β_N versus l_i space of NSTX. Blue is below the no-wall limit and red is above.

operation of NSTX, which is supported by a complete lack of observed sawtooth oscillations in these plasmas.

II.A. Stability versus β_N and l_i

Figure 1 shows the β_N versus l_i space of nearly five thousand experimental equilibria from 350 NSTX discharges, with the color of each point indicating the DCON calculated $\delta W_{\text{no-wall}}^{n=1}$. One can see that the previously defined no-wall limit [25] shown with the solid lines, $\beta_N = 4.3$ above $l_i \approx 0.64$ and $\beta_N/l_i = 6.7$ from $l_i \approx 0.4$ to 0.64 , does a good job describing the location of the no-wall limit in this data set. Naturally, there is some overlapping range as ideal stability is influenced by more parameters than just β_N and l_i , such as pressure peaking ($p_0/\langle p \rangle$) [7, 48] and aspect ratio [28, 49, 50], as will be discussed. Also, no restriction of plasma parameters was performed when plotting versus one parameter (i.e. when β_N versus aspect ratio is presented in the next section, other factors are changing with aspect ratio, such as field strength, which also may be important). Finally, we note that the red points have been plotted on top of the blue points, somewhat obscuring the extent of the overlapping range.

Each of the colored points plotted in figure 1 represents a stable experimental equilibrium point from NSTX, so it is evident that the device is able to operate well above the ideal MHD no-wall stability limit.

To obtain a better estimate of the $n = 1$ no-wall limit, we can examine the same data plotted as $-\delta W_{\text{no-wall}}^{n=1}$ versus β_N for $l_i \gtrsim 0.64$ (figure 2(a)) and versus β_N/l_i for $l_i \lesssim 0.64$ (figure 2(b)). Included on the plot are rough curve fits given by $\delta W_{\text{no-wall}}^{n=1} = 2(1 - (\beta_N/(6.7l_i))^3)$ for low l_i and $\delta W_{\text{no-wall}}^{n=1} = 2(1 - (\beta_N/4.3)^6)$ at high l_i . The dependency of $\delta W_{\text{no-wall}}^{n=1}$ on β_N/l_i will be combined in section II.C with similar dependencies on pressure peaking and aspect ratio to provide a better estimate of the no-wall beta limit.

Here one can also get a better sense of the overlap that is difficult to see in figure 1. For example, in figure 2(b) there are a number of computed ideal-unstable points (red) down

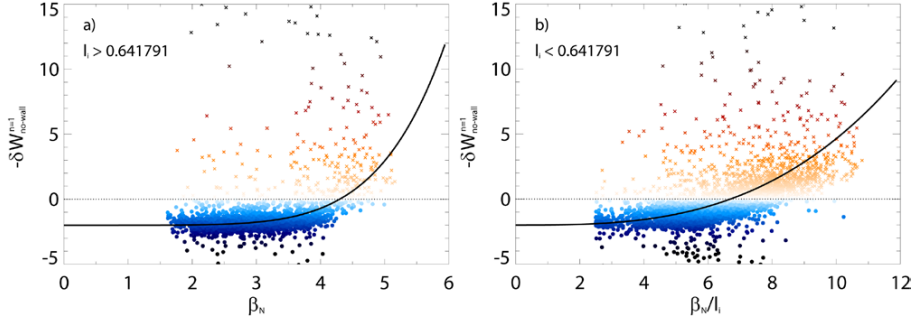


Figure 2. $-\delta W_{\text{no-wall}}^{n=1}$ versus (a) β_N for $l_i \gtrsim 0.64$ and (b) versus β_N/l_i for $l_i \lesssim 0.64$.

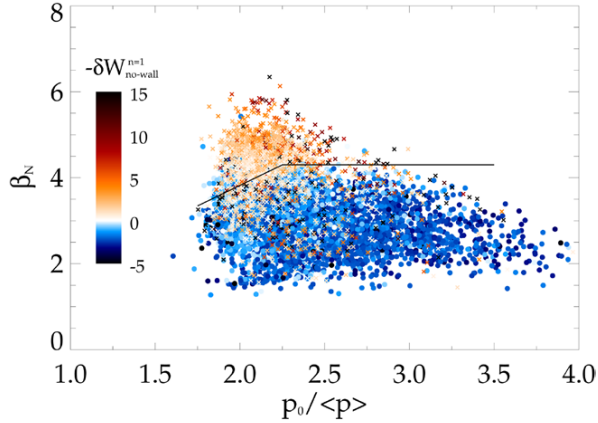


Figure 3. The β_N versus $p_0/\langle p \rangle$ space of NSTX. Blue is below the no-wall limit and red is above.

to $\beta_N/l_i \approx 4.5$ (which can be seen in figure 1) and ideal-stable points (blue) up to $\beta_N/l_i \approx 8$ (which are obscured).

II.B. Stability versus pressure peaking and aspect ratio

The β_N versus pressure peaking space in NSTX (figure 3) is fairly similar to the β_N versus l_i space, as might be expected since there is an experimental correspondence between broadened pressure and broadened current profiles (lower l_i), as is evident in figure 4. As was shown in figures 1 and 3, broad profiles generally allowed access to higher β_N in NSTX, but also lowered the no-wall beta limit, so that plasmas with low l_i and pressure peaking can be experimentally stable well above the no-wall limit.

If similar plots to those in figure 2 were made, we would find the approximate dependencies: $\delta W_{\text{no-wall}}^{n=1} = 2(1 - (\beta_N/(1.91p_0/\langle p \rangle))^3)$ for low $p_0/\langle p \rangle < 2.25$ and $\delta W_{\text{no-wall}}^{n=1} = 2(1 - (\beta_N/4.3)^6)$ at high $p_0/\langle p \rangle > 2.25$ (as at high l_i). One should also note that in addition to the no-wall beta limit, which increases as pressure peaking increases up to 2.25, there is an operational limit on β_N which decreases as pressure peaking increases above this point, as can be seen by the envelope of the experimental equilibria [27, 28].

The aspect ratio in NSTX ranged roughly from 1.3–1.6 in this database, which is achieved by changes in the plasma shape (see, for example, figures 20 and 21 of [28]). The ideal

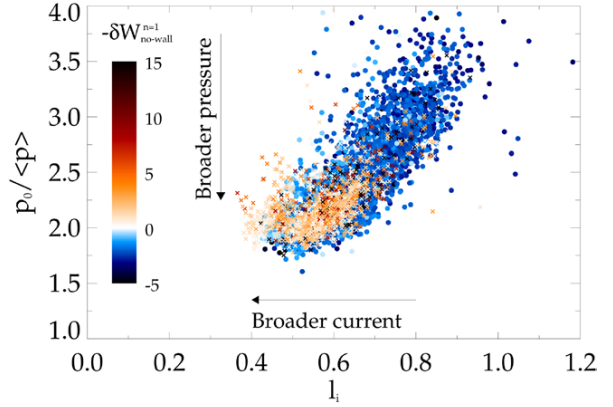


Figure 4. The $p_0/\langle p \rangle$ versus l_i space of NSTX. Blue is below the no-wall limit and red is above.

$n = 1$ no-wall beta limit decreases with increasing aspect ratio [49, 50, 52], $A = R_0/a$, where R_0 and a are the major and minor radii of the plasma, respectively. This property has been previously computed for NSTX [28], and is shown here with a much larger sample of equilibria in figure 5. Here we find a somewhat greater decrease with aspect ratio (the solid line, given by $\beta_N/(A^{-1} - 0.4) = 14$) than the approximate no-wall limit found previously in [51] (dashed line), which was itself somewhat smaller than previously expected from [50]. The corresponding fit for $\delta W_{\text{no-wall}}^{n=1}$ is $2(1 - (\beta_N/(14(A^{-1} - 0.4)))^3)$.

II.C. No-wall limit estimate

It is useful for purposes of disruption avoidance to have a real-time estimate of the no-wall limit, rather than running ideal stability codes after the discharges. This can be achieved by relying on quantities from real-time equilibrium reconstruction [53, 54]. As an example, if we combine the dependencies of $\delta W_{\text{no-wall}}^{n=1}$ on β_N/l_i , $\beta_N/(p_0/\langle p \rangle)$, and A at low l_i and low $p_0/\langle p \rangle$, we find: $\delta W_{\text{no-wall}}^{n=1} = F = 2 - \frac{2}{3}\beta_N^3((6.7l_i)^{-3} + (1.91p_0/\langle p \rangle)^{-3} + (14(A^{-1} - 0.4))^{-3})$. The zero-crossing of $\delta W_{\text{no-wall}}^{n=1}$ is the no-wall limit, and solving for $\beta_{N,\text{no-wall}}^{n=1}$ we find that the following estimate can be made for the no-wall beta limit based on equilibrium quantities: $\beta_{N,\text{no-wall}}^{n=1} = 3^{\frac{1}{3}}((6.7l_i)^{-3} + (1.91p_0/\langle p \rangle)^{-3} + (14(A^{-1} - 0.4))^{-3})^{-\frac{1}{3}}$.

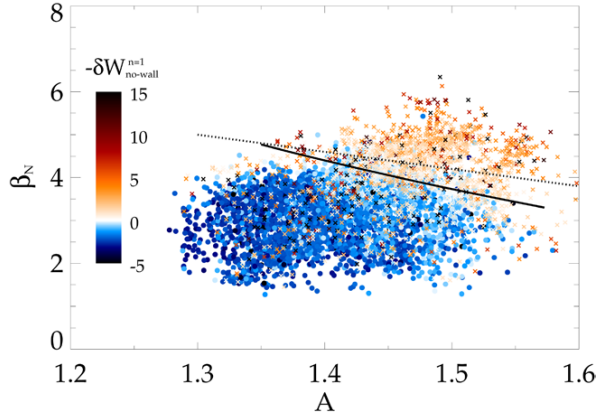


Figure 5. The β_N versus aspect ratio space of NSTX. Blue is below the no-wall limit and red is above. The dashed line in the approximate no-wall limit found in [51], while the solid line represents the current analysis.

We can then determine the error on that estimation by using the Gaussian width of the zero-crossing. We have found that the DCON calculations resulting in $|\delta W_{\text{no-wall}}^{n=1}| < 0.1$ have an average of $F = 0.04$ and a standard deviation of 0.74, which translates into almost zero offset and an error on the $\beta_{N,\text{no-wall}}^{n=1}$ estimation of roughly +11% and -14%. A similar analysis for the previous, simpler expression of $\beta_{N,\text{no-wall}}^{n=1} = 6.7l_i$ (with $F = 2(1 - (\beta_N/(6.7l_i))^3)$) showed a similar spread in the estimation ($F = 0.54 \pm 0.84$ giving error on $\beta_{N,\text{no-wall}}^{n=1}$ of +11%, -17%), but in that case there was also an offset such that $\beta_{N,\text{no-wall}}^{n=1} = 6.7l_i$ gives about 10% too low of an estimate compared to the full DCON analysis. Note that these calculations are computed using equilibrium reconstructions computed after the discharge rather than in real-time, the implications of which will be discussed presently.

To look at one specific example, in figure 6 β_N versus time is plotted for NSTX discharge 138556. In frame (a) the quantities were calculated using real-time equilibrium reconstruction, and in frame (b) with post-processed equilibrium reconstruction. The $\beta_{N,\text{no-wall}}^{n=1} = 6.7l_i$ limit is shown in red, $\beta_{N,\text{no-wall}}^{n=1} = 14(A^{-1} - 0.4)$ in green, and $\beta_{N,\text{no-wall}}^{n=1} = 1.9111(p_0/\langle p \rangle)$, which was not available in real-time, in blue. The composite estimate with +11%, -14% error bars is shown with the dashed black line and the grey area.

In both cases the original estimate of $\beta_{N,\text{no-wall}}^{n=1} = 6.7l_i$ is pretty close to the estimate that takes pressure peaking and aspect ratio into account, although both of those considerations tend to increase the no-wall limit estimate. The DCON calculated $-\delta W_{\text{no-wall}}^{n=1}$ versus time for the same discharge is plotted in figure 6(c). Here we see the zero-crossings at about 0.36 s and 1.05 s, which both roughly agree with the composite no-wall limit estimates, although the present real-time $\beta_{N,\text{no-wall}}^{n=1} = 6.7l_i$ (red) underestimates the no-wall limit slightly compared to both the post-processed equilibrium estimates and the DCON calculation, consistent with the statistical 10% offset previously discussed.

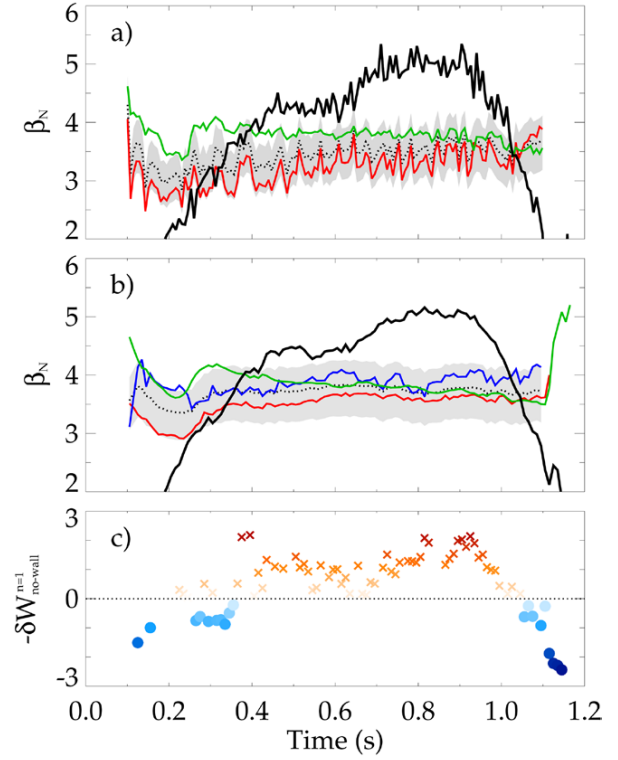


Figure 6. β_N versus time for NSTX discharge 138556 from (a) real-time and (b) post-processed equilibrium reconstruction. The $\beta_{N,\text{no-wall}}^{n=1} = 6.7l_i$ limit is shown in red, $\beta_{N,\text{no-wall}}^{n=1} = 1.9111(p_0/\langle p \rangle)$ in blue and $\beta_{N,\text{no-wall}}^{n=1} = 14 * (A^{-1} - 0.4)$ in green. The composite estimate with error bars is shown with the dashed black line and the grey area. (c) $-\delta W_{\text{no-wall}}^{n=1}$ versus time for the same discharge, calculated by DCON.

II.D. Ideal stability implications for NSTX-U

The ideal stability for projected NSTX-U [52] (the upgrade to NSTX) equilibria has been explored in the parameter space of β_N versus $p_0/\langle p \rangle$ previously, where a no-wall limit of $\beta_N \approx 3.5-4$ was found [51]. An even smaller no-wall limit in NSTX-U would be consistent with its somewhat larger aspect ratio (for example, for $A = 1.7$, $\beta_{N,\text{no-wall}}^{n=1} = 2.6$ is implied by the scaling in figure 5). This presently proposed scaling of $\beta_{N,\text{no-wall}}^{n=1}$ on aspect ratio will be further tested and refined by NSTX-U experiments. NSTX-U will also have new off-axis neutral beams that can potentially broaden the current, pressure, and plasma rotation profiles [51]. Broadened pressure [51, 55] and current [56] profiles can be beneficial in raising the ideal-wall beta limit, but they can also lower the no-wall limit, opening up a large β_N range in between them. Consequently, RWM stability will be of utmost importance to assure high-performance operation of NSTX-U. However, modifications to ideal stability by kinetic effects [20] (as will be discussed in section III), and active control of resistive wall modes [16] should continue to enable passively and actively stable operation in this range.

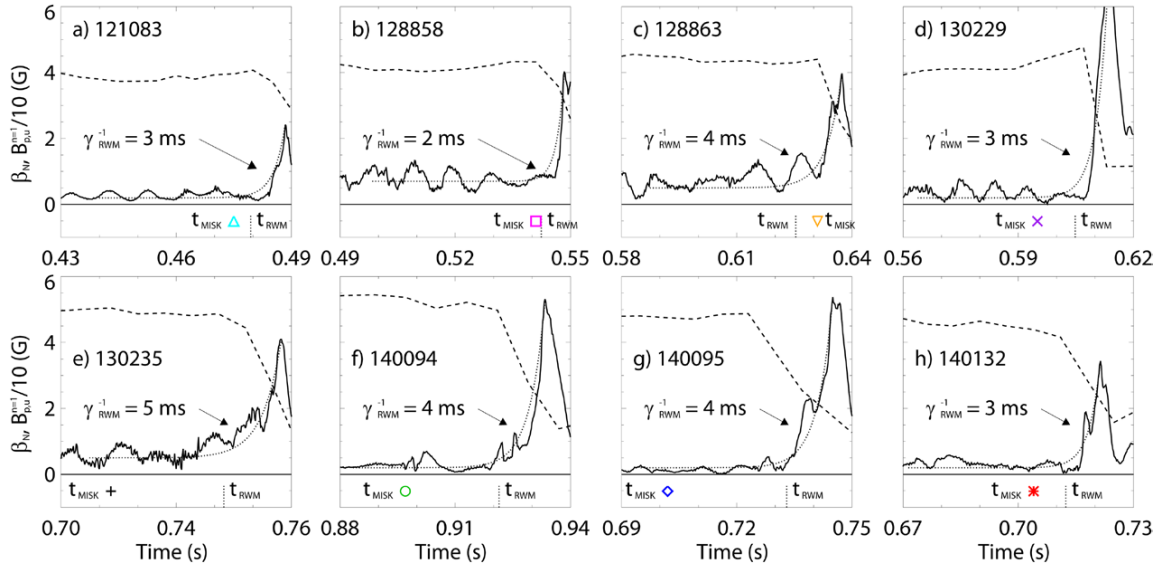


Figure 7. Eight NSTX discharges with an unstable RWM, showing β_N (dashed) and $n = 1$ magnetic field measured on the upper poloidal magnetic sensors, $B_{p,u}^{n=1}$ (solid), versus time. In each case an exponential is fit to $B_{p,u}^{n=1}$, which defines γ_{RWM}^{-1} and t_{RWM} is defined as $3\gamma_{RWM}^{-1}$ times before the measured peak in $B_{p,u}^{n=1}$. Also on the bottom panel are the times of the last MISK analysis for each discharge, indicated by the same symbols used in figures 8 and 9.

III. Modifications to ideal stability by kinetic effects

Clearly, tokamak fusion plasmas can operate stably above the ideal MHD no-wall limit (all red points in the previous plots are stable experimental equilibria points). Experiments in NSTX have previously shown that this is because the energy that would otherwise cause the RWM to grow is instead dissipated into particle motions via resonances with the plasma rotation [6, 20, 31, 37, 41]. To determine RWM marginal stability for use in experimental disruption avoidance, ideal stability limits like those calculated in the first part of this paper need to be modified by kinetic effects in order to reproduce experimental marginal stability points. Specifically, reduced stability models could be developed that could employ real-time measurements (of rotation, for example) and actuation (rotation control via magnetic braking or changing neutral beam sources) to detect approaches to marginal stability and return the plasma to a more stable state.

Here we examine the stability trajectories of several NSTX experimental RWM unstable discharges to validate the kinetic stability calculations of the marginal point with the MISK code, and to explore the effects of rotational resonances, energetic particles, and modification to the eigenfunction in more detail.

III.A. NSTX experiments reaching kinetic RWM marginal stability

Eight NSTX discharges with unstable RWMs are shown in figure 7. In each case an exponential is fit to the $n = 1$ magnetic field measured on the upper poloidal magnetic sensors $B_{p,u}^{n=1}$, which defines the growth time γ_{RWM}^{-1} . For these cases the growth times were 2–5 ms in each case. We then also define

the time of the beginning of unstable RWM growth, t_{RWM} , as beginning $3\tau_w$ times before the measured peak in $B_{p,u}^{n=1}$. One can see that this definition generally captures both the beginning time of the experimentally measured growth in magnetic field and the collapse of the plasma β . Theoretically, at t_{RWM} the growth rate of the RWM, γ , is changing from negative (damped) to positive (growing). Also indicated in figure 7 are the times of the latest equilibria from EFIT for each discharge that will be analyzed for stability by the MISK code. Generally these come before t_{RWM} due to the availability of equilibria before the collapse of the plasma beta which successfully run through the ideal stability PEST code, although in one case (frame c) the latest time is after t_{RWM} . These eight time points, t_{MISK} , will be analyzed in depth later, but they are not the only time points in these discharges that will be analyzed; earlier times in each discharge, not indicated here, were analyzed with MISK as well.

III.B. MISK calculations

As noted in the introduction, the MISK code calculates the growth rate of the RWM with kinetic modifications to ideal stability. The PEST code provides the eigenfunction, the fluid δW terms, and other quantities. Both codes use the EFIT equilibrium reconstruction for NSTX that includes thermal and energetic particle equilibrium pressures.

Figure 8 shows MISK calculated growth rates versus time before an unstable RWM, both normalized by the wall time. Note that in figure 8(a) the dominant rotational kinetic resonances are included, while in figure 8(b) the mostly non-resonant influence of energetic particles is also included (the effect of energetic particles will be discussed in more detail in section III.B.1). The eight trajectories of calculated stability

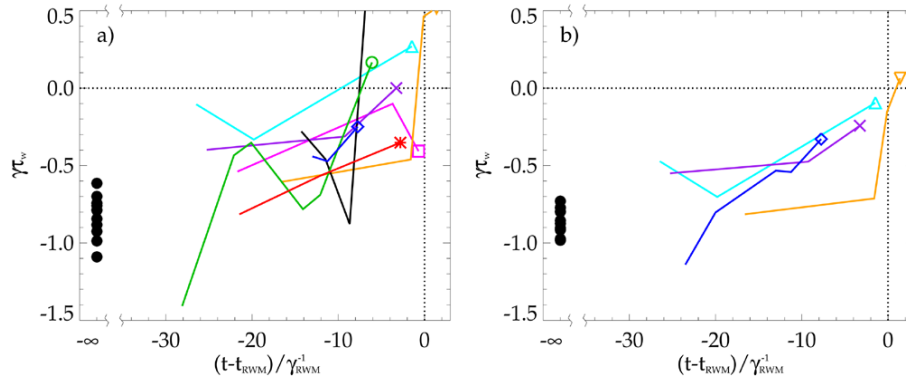


Figure 8. MISK calculated normalized growth rates versus normalized time before an unstable RWM (a) without energetic particle effects, and (b) with energetic particle effects. The points on the left side at ‘infinite’ time are from stable discharges where no RWM occurs. The eight trajectories toward instability, ending at the symbols, are for the same eight discharges as in figures 7 and 9.

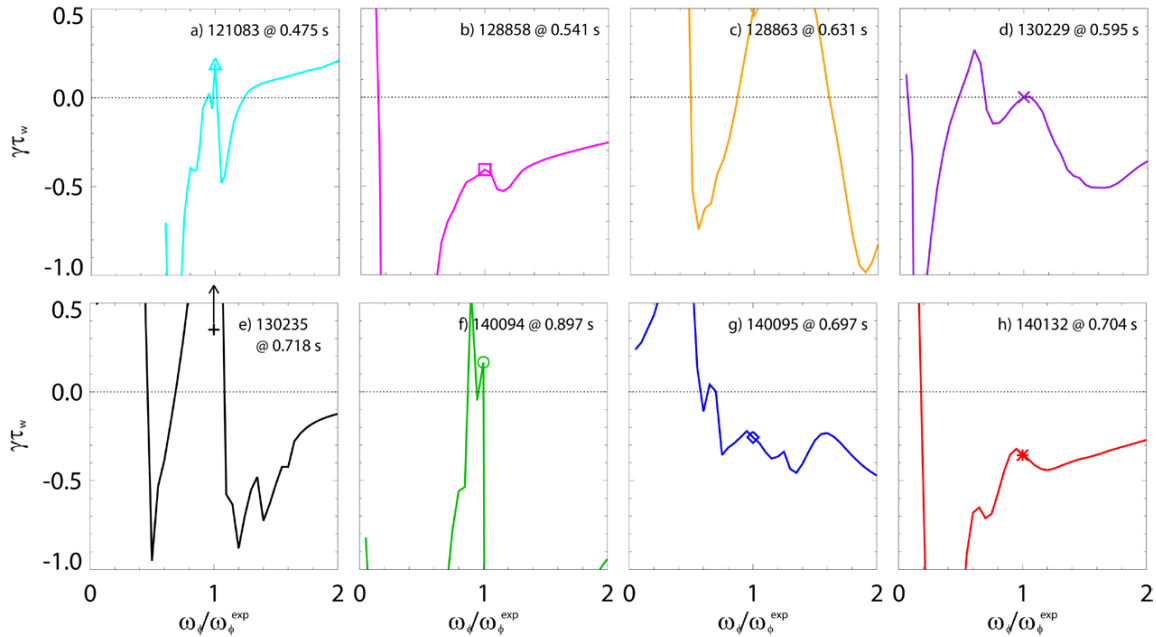


Figure 9. MISK analysis of eight NSTX discharges at the times indicated which are close to the RWM unstable time (see figure 7). Shown are calculated normalized growth rate versus scaled experimental plasma rotation. The calculation with the experimental rotation profile ($\omega_{\phi}/\omega_{\phi}^{\text{exp}} = 1$) is indicated by the symbols (also used in figures 7 and 8).

versus time in figure 8 are for the same eight discharges as in figures 7 and 9, with the symbols indicating the latest equilibrium used for MISK calculation, which are shown by t_{MISK} in figure 7 and will be analyzed in more depth, including variation in rotation in figure 9. In addition to the end time point, 2, 3, or in one case 7 time points earlier in each discharge were also analyzed, for a total of 31 equilibria in these eight discharges. One can see that in each case, the calculations trend towards instability ($\gamma\tau_w = 0$) as the time approaches the time in the experiment when the RWM instability begins to grow. Not all the discharges trend towards instability monotonically, although generally one would not expect that they would. As profiles change, kinetic RWM stabilization physics allows that discharges could become more stable before becoming less stable again leading up to the instability. Some of the discharges with the largest variation in figure 8(a) (130235, in

black, and 140094, in green) will be shown in figure 9 to have a large predicted stability gradient with rotation. Such cases may help to define the required equilibrium and other input accuracy for future analysis of real-time disruption prediction. Overall, MISK mainly predicts the RWM is slightly damped, as it should be, and is tending toward marginal stability within the time period of about 20 growth times before experimental RWM growth begins (approximately 60 ms, or the total time scales covered by the width of each frame of figure 7).

Additionally, MISK stability calculations for eleven time points from three discharges (taken from the same NSTX experiments) that remained stable to the RWM are also shown, on the left side of figure 8 (labeled as ‘ $-\infty$ ’ on the abscissa). Although in theory these discharges could have approached marginal RWM stability at some time during their high β phases and then returned to greater stability, that scenario was

not captured by this set of MISK calculations. Instead, all of the equilibria analyzed were predicted to be robustly stable to the RWM, with $\gamma\tau_w < -0.7$ for all but one case, an average value of $\gamma\tau_w = -0.83$, and no discernable trends versus time in each discharge. This is in contrast to the eight discharges which eventually went unstable in which only one of the 24 equilibria within about $20\tau_w$ of the unstable RWM fell below a $\gamma\tau_w$ of -0.6 . In practical terms, this means that roughly on the time scales shown by the frames of figure 7, MISK is indicating these discharges are close to marginal stability (and getting closer with time), especially when compared to three control cases in which no unstable RWM occurs.

If these calculations could have been performed in real time, they could have been used in a control system to indicate the approach of marginal stability. Of course, full MISK calculations can not be performed in real time, but simplified model calculations with comparison to experiment will be researched as a next step to the present analysis for this purpose [31].

III.B.1. Energetic particles. Energetic particles, such as neutral beam injection fast ions in NSTX, are theoretically expected to contribute to RWM stability as well [41, 57]. By using an anisotropic slowing-down distribution function for these particles, MISK can calculate their kinetic stability contribution. However, this is somewhat more complicated than the thermal particle calculation because the distribution function and the profiles that define it (two out of three of energy, density, and pressure must be supplied [41, 58]) are not measured directly. Here we used an anisotropic distribution function which approximates the beam injection angle and spread in NSTX (for an example of the sensitivity of the energetic particle calculation between an isotropic and anisotropic distribution, see figure 8 of [41]). For the profiles we used a consistent procedure where we used an energetic particle density profile that was broader than the classical-based TRANSP/NUBEAM profile (less peaked in the core, but consistent with the TRANSP/NUBEAM profile towards the edge), and which provides a pressure that is more consistent with the equilibrium reconstruction. This is consistent with the fact that our TRANSP/NUBEAM calculations assumed classical processes only (no anomalous fast ion diffusion), but the discharges exhibited low and high frequency Alfvén activity, which are known to cause a redistribution (i.e. flattening) of the fast ion pressure profile (also noted by Menard *et al* [34]). The resulting $\gamma\tau_w$ with thermal and energetic particle effects included is shown for half of the analyzed discharges in figure 8(b). One can see that the energetic particles are stabilizing and that they roughly give an increment from zero to -0.4 in $\gamma\tau_w$.

III.B.2. Rotation profile effect. Toroidal plasma rotation is the leading order effect on RWM kinetic plasma stability [19–21, 31, 41, 59, 60]. The end points of the MISK calculation trajectories (times close to the RWM unstable time) were analyzed in further detail to determine the sensitivity of each equilibrium to plasma rotation. This was accomplished by taking the

experimental rotation profile (ω_ϕ^{exp}) and scaling it to higher and lower values in the calculation. The results are shown in figure 9. In some of the cases shown, the experimental rotation profile sits very near to a local maxima in predicted growth rate (some more extreme than others), which could indicate the least stable ‘intermediate’ rotation that occurs between resonances with the ion bounce frequencies at higher rotation and precession frequency at low rotation. This has been previously identified as a cause of RWM instability in NSTX [20]. One exception seems to be 140095, in which case the code predicts RWM instability with a modest decrease in plasma rotation (approximately 30%), which is consistent with the observation of instability in this discharge a short time later, because the plasma rotation continued to drop after the analyzed time.

III.B.3. Sensitivity to the eigenfunction. Like the profiles of the energetic particles, the magnetic structure of the mode, known as the mode eigenfunction, is also not directly measured, but rather it is calculated and used in the stability calculation. In MISK code calculations the RWM eigenfunction is first obtained from PEST by steadily decreasing an ideal conformal wall radius until the point where the ideal kink is just stabilized by the wall, i.e. the marginally stable ideal kink eigenfunction [35, 40]. Then this eigenfunction is used for all subsequent analysis—first to obtain the fluid terms δW_b and δW_∞ from PEST with a realistic NSTX wall and no wall, respectively, and then also in the MISK calculation itself, where ξ_\perp appears. When the plasma is above the no-wall limit, as is always the case in the equilibria analyzed here, the realistic NSTX wall is necessary to convert the ideal kink into the more slowly growing RWM, which itself would be unstable if not for the kinetic effects calculated by MISK.

In one approach, changes to the eigenfunction by kinetic effects can be self-consistently calculated [18, 61]. In the so-called perturbative approach, used here, the eigenfunction is not changed by the kinetic effects and in the linear RWM growth phase there is no need to evoke non-linear effects to explain the experimental marginal point. The present analysis shows that MISK calculations that use the linear ideal eigenfunction yield close agreement between the computed kinetic RWM marginal stability boundary and the experimental RWM marginal stability points.

Here, we examine the sensitivity of MISK calculations to changes to the eigenfunction in a systematic way. One way of doing that is to examine the change to $\gamma\tau_w$ from a change to a more external eigenfunction, which can be obtained by moving the ideal conformal wall radius outward slightly in PEST. To do this systematically, we chose to compare the original results to those with an eigenfunction obtained by moving the wall out by a small amount $\Delta r/a = 0.06$. It should be noted that for plasmas closer to the ideal wall limit that had required a closer conformal wall to obtain the marginal eigenfunction (say $r/a = 0.25$), changing the wall by $\Delta r/a = 0.06$ (to $r/a = 0.31$) is a more substantial change than for plasmas farther from the ideal wall limit ($r/a = 0.5 \rightarrow 0.56$, for example). One example of the change in the eigenfunction

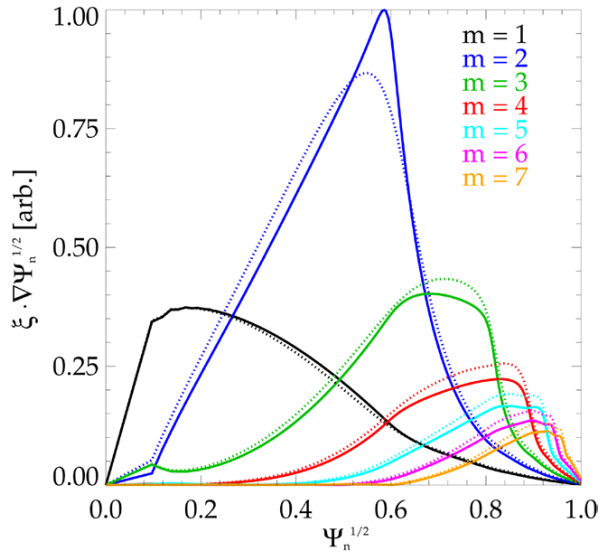


Figure 10. The first seven poloidal Fourier harmonics of the normal displacement for the marginally stable ideal kink mode (solid) and with the wall moved outward by $\Delta r/a = 0.06$ (dashed) for NSTX discharge 130229 at 0.595 s. The eigenfunctions are normalized so that the peaks of the $m = 1$ components are the same.

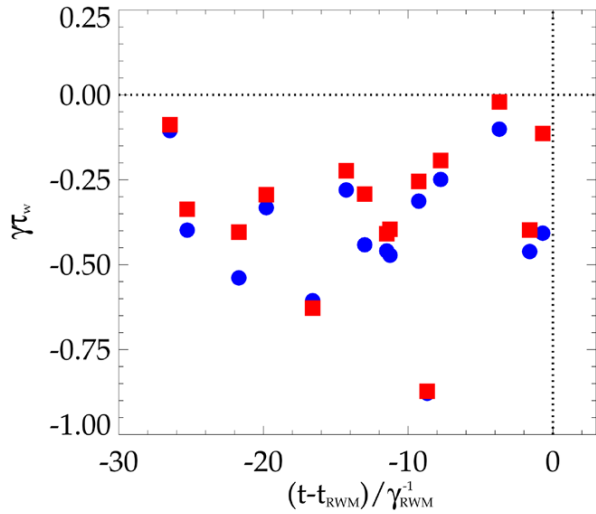


Figure 11. The effect of changing the eigenfunction used in MISC analysis to a slightly more external eigenfunction is shown by the change vertically from the blue circles (original calculation) to the red squares.

from this procedure is shown in figure 10, which shows that it becomes slightly more external in nature, but does not substantially change the poloidal mode spectrum.

The results of changing the eigenfunction are shown in figure 11 for a subset of 15 calculations from the set shown previously in figure 8(a). The blue circles, which are the original calculations have moved vertically to the red squares, which are with the slightly changed (more external) eigenfunctions. One can see that this type of change to the eigenfunction has generally had a relatively small, but consistently destabilizing, effect on the calculated growth rate. Moving the

wall by $\Delta r/a = 0.06$ changed the γ_{RWM} on average by 0.075, with a standard deviation of about the same value (0.074). More significant changes to the eigenfunction can have larger effects on the calculation of γ_{RWM} which are no longer supported by the experimental results, for example predicting significant instability for plasmas that are just approaching marginal stability.

IV. Conclusions

To explain experimental passive stability above the no-wall limit modifications to ideal stability due to kinetic effects need to be included. The ideal stability of NSTX was explored with the DCON code for a large database of equilibria. A formulation of the no-wall beta limit that can be used in real-time for disruption prediction was computed. This estimate takes into account pressure peaking and aspect ratio and is in line with previous estimates of the no-wall beta limit in the β_N versus l_i operating space, although the decrease in the no-wall limit with aspect ratio is somewhat larger than previously estimated. This could have implications for the larger aspect ratio NSTX-U, in that a larger percentage of discharges will be above the no-wall limit and potentially subject to resistive wall mode instabilities than in NSTX.

Calculations of the resistive wall mode growth rate through kinetic modifications to ideal stability with the MISC code have been previously compared to experiments from multiple devices and benchmarked against other codes. Here MISC calculations are now further validated by detailed comparison to experimental results from NSTX. Eight discharges with growing, unstable RWMs were analyzed and growth rates were calculated for multiple equilibria from each of those eight discharges as well as for several discharges which did not have an unstable RWM, for comparison. In each case the calculations approach marginal stability as the experiments do, though not always monotonically (which may, of course, be a true feature of these discharges which are changing in time). Energetic particle effects generally add a degree of stability to the calculations. Resistive wall modes in NSTX are shown to often go unstable at a local minima in stability versus plasma rotation, in between stabilizing rotational resonances at higher and lower rotation. The sensitivity to the eigenfunction is also explored by making the eigenfunction slightly more external than the usual procedure, which results in a slightly less stable growth rate. The present research represents a required new stage of analysis moving toward creating an experimentally validated, reduced model of kinetic RWM stability determination for use in real-time instability prediction.

Acknowledgments

The authors would like to thank S Kaye for his careful reading and editing of the manuscript. This research was supported by the US Department of Energy under contracts: DE-FG02-99ER54524 (Columbia University) and DE-AC02-09CH11466 (Princeton Plasma Physics Laboratory).

References

- [1] Boozer A.H. 2012 *Phys. Plasmas* **19** 058101
- [2] Bondeson A. and Ward D. 1994 *Phys. Rev. Lett.* **72** 2709
- [3] Strait E., Taylor T., Turnbull A., Ferron J., Lao L., Rice B., Sauter O., Thompson S. and Wroblewski D. 1995 *Phys. Rev. Lett.* **74** 2483
- [4] Chu M.S. and Okabayashi M. 2010 *Plasma Phys. Control. Fusion* **52** 123001
- [5] Ono M. et al 2000 *Nucl. Fusion* **40** 557
- [6] Sabbagh S.A. et al 2010 *Nucl. Fusion* **50** 025020
- [7] Sabbagh S.A. et al 2002 *Phys. Plasmas* **9** 2085
- [8] Hole M.J. et al 2005 *Plasma Phys. Control. Fusion* **47** 581
- [9] Sabbagh S.A. et al 2006 *Nucl. Fusion* **46** 635
- [10] Hole M.J., Wilson H.R., Abeysuriya R. and Larson J.W. 2010 *Plasma Phys. Control. Fusion* **52** 125005
- [11] Troyon F., Gruber R., Saurenmann H., Semenzato S. and Succi S. 1984 *Plasma Phys. Control. Fusion* **26** 209
- [12] Freidberg J. 2014 *Ideal MHD* (Cambridge: Cambridge University)
- [13] Sabbagh S.A. et al 1991 *Phys. Fluids B* **3** 2277
- [14] Lao L.L., Taylor T.S., Chu M.S., Chan V.S., Ferron J.R. and Strait E.J. 1992 *Phys. Fluids B* **4** 232
- [15] Ferron J.R., Lao L.L., Taylor T.S., Kim Y.B., Strait E.J. and Wroblewski D. 1993 *Phys. Fluids B* **5** 2532
- [16] Sabbagh S.A., Bell R.E., Menard J.E., Gates D.A., Sontag A.C., Bialek J.M., LeBlanc B.P., Levinton F.M., Tritz K. and Yuh H. 2006 *Phys. Rev. Lett.* **97** 045004
- [17] Hu B. and Betti R. 2004 *Phys. Rev. Lett.* **93** 105002
- [18] Liu Y., Chu M.S., Chapman I.T. and Hender T.C. 2008 *Phys. Plasmas* **15** 112503
- [19] Chapman I.T., Gimblett C.G., Gryaznevich M.P., Hender T.C., Howell D.F., Liu Y.Q. and Pinches S.D. 2009 *Plasma Phys. Control. Fusion* **51** 055015
- [20] Berkery J.W., Sabbagh S.A., Betti R., Hu B., Bell R.E., Gerhardt S.P., Manickam J. and Tritz K. 2010 *Phys. Rev. Lett.* **104** 035003
- [21] Reimerdes H., Berkery J.W., Lanctot M.J., Garofalo A.M., Hanson J.M., In Y., Okabayashi M., Sabbagh S.A. and Strait E.J. 2011 *Phys. Rev. Lett.* **106** 215002
- [22] Chapman I.T. et al 2011 *Nucl. Fusion* **51** 073040
- [23] Yadykin D., Liu Y.Q. and Paccagnella R. 2011 *Plasma Phys. Control. Nucl. Fusion* **53** 085024
- [24] Sabbagh S.A. et al 2001 *Nucl. Fusion* **41** 1601
- [25] Sabbagh S.A. and The NSTX Team 2013 *Nucl. Fusion* **53** 104007
- [26] Menard J.E. et al 2003 *Nucl. Fusion* **43** 330
- [27] Sabbagh S.A. et al 2004 *Nucl. Fusion* **44** 560
- [28] Gerhardt S.P. et al 2011 *Nucl. Fusion* **51** 073031
- [29] Gerhardt S.P. et al 2013 *Nucl. Fusion* **53** 043020
- [30] Reimerdes H., Chu M.S., Garafalo A.M., Jackson G.L., La Haye R.J., Navratil G., Okabayashi M., Scoville J.T. and Strait E.J. 2004 *Phys. Rev. Lett.* **93** 135002
- [31] Berkery J.W. et al 2014 *Phys. Plasmas* **21** 056112
- [32] Wang Z.R., Lanctot M.J., Liu Y.Q., Park J.K. and Menard J.E. 2015 *Phys. Rev. Lett.* **114** 145005
- [33] Turco F., Turnbull A.D., Hanson J.M. and Navratil G.A. 2015 *Phys. Plasmas* **22** 022503
- [34] Menard J.E., Wang Z., Liu Y., Bell R.E., Kaye S.M., Park J. and Tritz K. 2014 *Phys. Rev. Lett.* **113** 255002
- [35] Hu B., Betti R. and Manickam J. 2005 *Phys. Plasmas* **12** 057301
- [36] Hu B., Betti R. and Manickam J. 2006 *Phys. Plasmas* **13** 112505
- [37] Berkery J.W., Sabbagh S.A., Betti R., Bell R.E., Gerhardt S.P., LeBlanc B.P. and Yuh H. 2011 *Phys. Rev. Lett.* **106** 075004
- [38] Berkery J.W., Betti R. and Sabbagh S.A. 2011 *Phys. Plasmas* **18** 072501
- [39] Berkery J.W., Betti R., Sabbagh S.A., Guazzotto L. and Manickam J. 2014 *Phys. Plasmas* **21** 112505
- [40] Berkery J.W., Liu Y.Q., Wang Z.R., Sabbagh S.A., Logan N.C., Park J.K., Manickam J. and Betti R. 2014 *Phys. Plasmas* **21** 052505
- [41] Berkery J.W., Sabbagh S.A., Reimerdes H., Betti R., Hu B., Bell R.E., Gerhardt S.P., Manickam J. and Podesta M. 2010 *Phys. Plasmas* **17** 082504
- [42] Reimerdes H. et al 2007 *Plasma Phys. Control. Fusion* **49** B349
- [43] Grimm R., Greene J. and Johnson J. 1976 Chapter: computation of the magnetohydrodynamic spectrum in axisymmetric toroidal confinement systems *Methods in Computational Physics* vol **16**, ed J. Killeen (New York: Academic) pp 253–80
- [44] Glasser A. and Chance M. 1997 *Bull. Am. Phys. Soc.* **42** 1848
- [45] LeBlanc B.P., Bell R.E., Johnson D.W., Hoffman D.E., Long D.C. and Palladino R.W. 2003 *Rev. Sci. Instrum.* **74** 1659
- [46] Group I.P.E. 1999 *Nucl. Fusion* **39** 2251
- [47] Huysmans G.T.A. 2005 *Plasma Phys. Control. Fusion* **47** 2107
- [48] Howl W., Turnbull A.D., Taylor T.S., Lao L.L., Helton F.J., Ferron J.R. and Strait E.J. 1992 *Phys. Fluids B* **4** 1724
- [49] Menard J.E., Jardin S.C., Kaye S.M., Kessel C.E. and Manickam J. 1997 *Nucl. Fusion* **37** 595
- [50] Menard J.E., Bell M.G., Bell R.E., Gates D.A., Kaye S.M., LeBlanc B.P., Maingi R., Sabbagh S.A., Soukhanovskii V. and Stutman D. 2004 *Phys. Plasmas* **11** 639
- [51] Gerhardt S.P., Andre R. and Menard J.E. 2012 *Nucl. Fusion* **52** 083020
- [52] Menard J.E. and The NSTX Team 2012 *Nucl. Fusion* **52** 083015
- [53] Ferron J.R., Walker M.L., Lao L.L., John H.E.S., Humphreys D.A. and Leuer J.A. 1998 *Nucl. Fusion* **38** 1055
- [54] Gates D. et al 2006 *Nucl. Fusion* **46** 17
- [55] Ferron J.R. et al 2013 *Phys. Plasmas* **20** 092504
- [56] Turnbull A.D., Taylor T.S., Chu M.S., Miller R.L. and Lin-Liu Y.R. 1998 *Nucl. Fusion* **38** 1467
- [57] Liu Y.Q., Chapman I.T., Graves J.P., Hao G.Z., Wang Z.R., Menard J.E., Okabayashi M., Strait E.J. and Turnbull A. 2014 *Phys. Plasmas* **21** 056105
- [58] Liu Y. et al 2010 *Plasma Phys. Control. Fusion* **52** 104002
- [59] Liu Y., Chu M.S., Gimblett C.G. and Hastie R.J. 2008 *Phys. Plasmas* **15** 092505
- [60] Wang Z.R., Guo S.C. and Liu Y.Q. 2012 *Phys. Plasmas* **19** 072518
- [61] Liu Y., Chu M.S., Chapman I.T. and Hender T.C. 2009 *Nucl. Fusion* **49** 035004